Modern Physics Letters B
Vol. 29, No. 24 (2015) 1550140 (14 pages)

DOI: 10.1142/S0217984915501407

Theoretical investigation of elastic and phononic properties of $Zn_{1-x}Be_xO$ alloys

F. Elhamra*, S. Lakel*,†,¶, M. Ibrir‡, K. Almi* and H. Meradji§

*Laboratory of Physical Materials,
University of Laghouat – BP 37G, Laghouat, Algeria
†Laboratoire de Matériaux Semi Conducteurs et Métalliques "LMSM",
Université de Biskra, Algeria
‡Department de Physique, Université de M'sila, Algeria
§Laboratoire de Physique des Rayonnements,
Université Badji Mokhtar, Annaba, Algeria
¶s.lakel@yahoo.fr

Received 28 November 2014
Revised 11 March 2015
Accepted 28 March 2015
Published 31 August 2015

Our calculations were conducted within density functional theory (DFT) and density functional perturbation theory (DFPT) using norm-conserving pseudo-potential and the local density approximation. The elastic constants of $Zn_{1-x}Be_xO$ were calculated, C_{11}, C_{33} and C_{44} increase with the increase of Be content, whereas the C_{12} shows a non-monotonic variation and C_{13} decreases when Be concentration increases. The values of bulk modulus B, Young's modulus E and shear modulus G increase with the increase of Be content. Poisson's ratio σ decreases with increased Be concentration. The ductility decreases with increasing Be concentration and the compressibility for $Zn_{1-x}Be_xO$ along c-axis is smaller than along a-axis. Phonon dispersion curves show that $Zn_{1-x}Be_xO$ is dynamically stable (no soft modes). Quantities such as refractive index, Born effective charge, dielectric constants and optical phonon frequencies were calculated as a function of the Be molar fraction x. The agreement between the present results and the known data that are available only for ZnO and BeO is generally satisfactory. Our results for $Zn_{1-x}Be_xO$ $(0 < x < 1)$ are predictions.

Keywords: $Zn_{1-x}Be_xO$; DFT; DFPT; lattice dynamics; phonon dispersion; Born effective charge.

1. Introduction

In recent years, ZnO has received considerable attention as a promising material for electronics, optics and optoelectronics due to the wide band gap (3.37 eV) and large excitation binding energy (60 meV) at room temperature.[1] References 1 and 2 have indicated the potential for development of ZnO-based ultraviolet (UV) LEDs for

¶Corresponding author.

applications such as solid state lighting and antimicrobial lamps. As recent years have shown, the importance of ZnO-based devices shall take advantage of quantum-well (QW) structures to optimize the device performance.[2] Fabrication of single and multiple ZnO-based QWs from ZnO/ZnMgO,[3] ZnO/ZnBeO,[4] CdZnO/ZnO,[5] and CdZnO/MgZnO (Ref. 6) on various substrates have already been demonstrated with different growth techniques for producing high-efficiency ZnO devices by changing band gaps which are larger or smaller than that of ZnO.

The element Be is commonly regarded as a promising doping in ZnO, mainly attributed to the same stable wurtzite structure of BeO and ZnO, a big band gap of BeO (10.6 eV), as well as the solubility of Be in ZnO.[7] Besides, ZnO and its ternary alloys, as piezoelectric semiconductors, have been used for high-frequency surface acoustic wave (SAW) devices in wireless communication systems due to their high acoustic velocities and large electromechanical coupling.[8,9] To the best of our knowledge, the elastic, vibrational and thermodynamic properties of this alloy are less studied. This fact poses an obstacle to our understanding of the transport properties, especially the thermal conductivity, which are of importance in the development of high quality optoelectronic devices.

The paper is organized as follows: In Sec. 2, we give a brief description of the computational details. Section 3 provides the results and discussion relating to structural and elastic properties of $Zn_{1-x}Be_xO$. Then the phonon properties of the $Zn_{1-x}Be_xO$ including phonon dispersion relations partial phonon densities of states, electronic (ε_∞) and static (ε_0) dielectric permittivity tensors and Born effective charge tensors are calculated using the density functional perturbation theory (DFPT) method. Finally, we present our conclusions.

2. Computational Methods

All the calculations are carried out using plane wave pseudo-potential method based on density functional theory (DFT),[10] implemented in the Cambridge Serial Total Energy Package (CASTEP) code.[11,12] The local density approximation (LDA) in CA–PZ function[13,14] is used to describe the exchange–correlation energy functional. The valence states of Be, Zn and O atoms are $2s^2$, $3d^{10}4s^2$ and $2s^22p^4$, respectively. The interaction between ion core and valence electron is described by norm-conserving pseudo-potential.[15] Two parameters that affect the accuracy of calculation are cutoff energy which determines the number of plane waves and the number of special k-points which are used for the Brillouin zone (BZ) integration. The plane wave cutoff energy in reciprocal space was taken as 600 eV. The BZ with Monkhorst–Pack scheme at special k-points[16] of $5 \times 5 \times 6$. Noting that structural optimizations carried out using Broyden–Fletcher–Goldfarb–Shanno (BFGS) minimization technique.[17] The tolerances for geometry optimization were set as the difference of total energy within 1.0×10^{-6} eV/atom. In order to simulate the ordered $Zn_{1-x}Be_xO$ alloys with wurtzite structure, we employed 16-atom $Zn_{8-x}Be_xO_8$ supercell, which corresponds to a $2 \times 2 \times 1$ supercell that is twice the

size of a primitive wurtzite unit cell in base plane direction and a single periodicity along the c-axis.

The lattice dynamic properties are calculated on the corresponding optimized crystal geometries. Born effective charge tensors, phonon frequencies and dielectric permittivity tensors are obtained as second-order derivatives of the total energy with respect to an external electric field or to atomic displacements within the framework of DFPT.[18]

3. Results and Discussion

3.1. *Structural and mechanical properties*

Firstly, we calculated the equilibrium structural parameters for the parent binary compound ZnO in the wurtzite (#186) structure. There are 16 atoms (8 Zn and 8 O) which correspond to a $2\times2\times1$ supercell. When we add the Be atom to the ZnO, in order to obtain $Zn_{1-x}Be_xO$, the most probable crystal structures, according to x content, for this ternary, we take some selected compositions ($x = 0.0$, 0.25, 0.5, 0.75, 1).

The calculated lattice constants for each x of the $Zn_{1-x}Be_xO$ alloys are summarized in Table 1, along with the other experimental and theoretical values available in the literature.[19–22]

The results for the ZnO and BeO are in good agreement with the experimental data[19,22] and other calculations.[20,21] In addition, the calculated structure parameters of $Zn_{0.75}Be_{0.25}O$, $Zn_{0.5}Be_{0.5}O$ and $Zn_{0.25}Be_{0.75}O$ are in agreement with

Table 1. Calculated lattice constants a and c of $Zn_{1-x}Be_xO$ after geometric optimization compared with available theoretical and experimental data.

Structures		a (Å)	c (Å)	c/a
ZnO	This work	3.278	5.285	**1.612**
	Other results	3.258[a]	5.220[a]	1.602[a]
		3.283[b]	5.309[b]	1.617[b]
		3.256[c]	5.256[c]	1.614[c]
$Zn_{0.75}Be_{0.25}O$	This work	**3.107**	**5.091**	**1.638**
	Other results	3.134[c]	5.076[c]	1.620[c]
$Zn_{0.5}Be_{0.5}O$	This work	**2.923**	**5.022**	**1.718**
	Other results	2.972[c]	4.990[c]	1.679[c]
$Zn_{0.25}Be_{0.75}O$	This work	**2.811**	**4.528**	**1.611**
	Other results	2.889[c]	4.675[c]	1.618[c]
BeO	This work	**2.614**	**4.255**	**1.628**
	Other results	2.698[d]	4.377[d]	1.624[d]
		2.764[c]	4.487[c]	1.623[c]

[a]Ref. 19, [b]Ref. 20, [c]Ref. 21, [d]Ref. 22.

theoretical work.[21] The results listed in Table 1 show that the lattice constants, a and c, decrease with increasing Be concentration. This phenomenon occurs because the atom radius of beryllium is smaller than that of zinc.

The elastic constants (C_{ij}) are important parameters that describe the response to an applied macroscopic stress and give important information concerning the nature of the forces exerting on solids. Besides, they can provide information on the phase stability and stiffness of materials.

The traditional mechanical stability conditions of the elastic constants, in hexagonal crystal, are known to be as follows 0 GPa:[23,24]

$$C_{11} > 0, \quad C_{11} - C_{12} > 0, \quad C_{44} > 0, \quad (C_{11} + C_{12})C_{33} - 2C_{13}^2 > 0\,. \tag{1}$$

The elastic properties of crystals have been the most extensively investigated in both experiment and theory. A number of equations for estimating the elastic and physical properties of hexagonal polycrystalline materials are presented in literature.[25,26] The bulk modulus (B), Voigt shear modulus G_V, Voigt bulk modulus B_V, Reuss shear modulus G_R and Reuss bulk modulus B_R are given by Refs. 27–29,

$$G_V = \frac{1}{5}(2C_{11} + C_{33} - C_{12} - 2C_{13}) + \frac{1}{5}(2C_{44} + C_{66})\,, \tag{2}$$

$$B_V = \frac{2}{9}\left(\frac{C_{11} + C_{12} + 2C_{13} + C_{33}}{2}\right), \tag{3}$$

$$B_R = \frac{1}{2(S_{11} + S_{33}) + 2(S_{12} + 2S_{13})}\,, \tag{4}$$

$$G_R = \frac{15}{4(2S_{11} + S_{33}) - 4(S_{12} + 2S_{13}) + 3(2S_{44} + S_{66})}\,. \tag{5}$$

Hill shear modulus B_H and bulk modulus G_H can be expressed as:[30]

$$B = B_H = \frac{B_V + B_R}{2}\,, \tag{6}$$

$$G = G_H = \frac{G_V + G_R}{2}\,. \tag{7}$$

The polycrystalline Young's modulus E and Poisson's ratio σ are then calculated from these elastic constants using the following relations:[27]

$$E = \frac{9BG}{3B + G}\,, \tag{8}$$

$$\sigma = \frac{3B - 2G}{2(3B + G)}\,. \tag{9}$$

Table 2 shows the results of elastic constants C_{11}, C_{12}, C_{13}, C_{33} and C_{44} for wurtzite $Zn_{1-x}Be_xO$ alloys as a function of Be concentration. We note that the values of elastic constants change continuously from those of ZnO to those of BeO as Be concentration increases from 0% up to 100%, although the overall trend can be formulated as follows: In the entire range of concentration x, the elastic constants

Table 2. The calculated elastic constants for $Be_xZn_{1-x}O$ compared with both theoretical and experimental data.

Structures		C_{11}	C_{12}	C_{13}	C_{33}	C_{44}
ZnO	This work	**190.62**	**120.84**	**111.80**	**194.70**	**30.20**
	Experiments	206.217[a]	118.117[a]	118[a]	211[a]	44.50[a]
	Calculations	227[b]; 217[c]	55[b]; 117[c]	93[b]; 121[c]	206[b]; 225[c]	49[b]; 50[c]
		215.7[d]	136.1[d]	122.7[d]	249.6[d]	38.6[d]
		191.16[e]	111.96[e]	85.63[e]	190.57[e]	36.89[e]
$Zn_{0.75}Be_{0.25}O$	This work	**232.08**	**121.65**	**117.3**	**281.32**	**54.63**
$Zn_{0.5}Be_{0.5}O$	This work	**233.20**	**89.28**	**98.61**	**433.81**	**71.96**
$Zn_{0.25}Be_{0.75}O$	This work	**294.17**	**125.97**	**105.38**	**391.31**	**88.44**
BeO	This work	**464.40**	**108.87**	**73.58**	**528.39**	**158.70**
	Experiments	460.6[f]	126.5[f]	88.5[f]	491.6[f]	147.7[f]
	Calculations	432.5[d]	135.8[d]	99.0[d]	474.1[d]	131.3[d]

[a]Ref. 31, [b]Ref. 32, [c]Ref. 33, [d]Ref. 34, [e]Ref. 35, [f]Ref. 36.

C_{11}, C_{33} and C_{44} increase with the increase of Be content, whereas C_{12} shows a non-monotonic variation and C_{13} decreases when Be concentration increases. Obviously, from the calculated values of C_{ij} in Table 2, the above restrictions are all satisfied, implying that $Zn_{1-x}Be_xO$ alloys as a function of Be concentration are mechanically stable.

The values of bulk and shear modulus B and G, Young's modulus E, Poisson's ratio σ, linear compressibility ratio K_c/K_a and ratio B/G for each x of $Zn_{1-x}Be_xO$ alloys are given in Table 3. It is apparent from Table 3 that the quantities B,

Table 3. Bulk and shear moduli B and G (all in GPa), Young's modulus E (all in GPa), Poisson's ratio σ, linear compressibility ratio k_c/k_a and ratio B/G.

Structures	ZnO	$Zn_{0.75}Be_{0.25}O$	$Zn_{0.5}Be_{0.5}O$	$Zn_{0.25}Be_{0.75}O$	BeO
B_V (GPa)	148.36	162.02	163.69	183.68	218.81
B_R (GPa)	148.26	161.02	161.38	182.01	218.67
B_H (GPa)	148.31	161.52	162.53	182.84	218.74
	160.2[a]	167.48[a]	177.84[a]	197.29[a]	223[a]
G_V (GPa)	32.71	58.84	83.27	95.06	179.11
G_R (GPa)	32.47	57.91	77.45	92.35	176.38
G_H (GPa)	32.59	58.37	80.36	93.70	177.74
	44[b]				176[c]
E (GPa)	90.65	156.28	206.04	240.09	419.58
	164[a], 111.2[d]				439.6[a]
σ	0.39	0.34	0.28	0.28	0.18
	0.349[e]				0.177[f]
B/G	4.24	2.77	1.96	1.95	1.23
K_c/K_a	1.14	0.73	0.37	0.73	0.94

[a]Ref. 34, [b]Ref. 37, [c]Ref. 38, [d]Ref. 39, [e]Ref. 40, [f]Ref. 41.

E and G increase with the increase of Be content. Poisson's ratio σ is a very important property for industrial applications. From Table 3, we can see that the Poisson's ratio decreases with increasing Be concentration. It is also known that a high (low) B/G value is associated with ductility (brittleness), and the critical value which separates ductile and brittle materials is about 1.75.[42] The ductility decreases with increasing Be concentration. The parameter K_c/K_a is employed, it expresses the ratio between linear compressibility coefficients.[43] We have calculated the ratio between linear compressibility coefficients K_c/K_a for a hexagonal crystal by $k_c/k_a = (C_{11} + C_{12} - 2C_{13})/(C_{33} - C_{13})$. The obtained information $K_c/K_a > 1$ demonstrates that the compressibility for ZnO along c-axis is larger than along a-axis and $K_c/K_a < 1$ shows that the compressibility for $Zn_{0.75}Be_{0.25}O$, $Zn_{0.5}Be_{0.5}O$, $Zn_{0.25}Be_{0.75}O$ and BeO along c axis is smaller than along a-axis.

3.2. *Lattice dynamic properties*

3.2.1. *Phonon dispersion and density of states*

The harmonic approximation is usually a typical description for the physics of phonon, in which the equation of motion takes the form of:[44]

$$\omega^2(k,l)e(k,l) = D(k)e(k,l)\,, \tag{10}$$

where $\omega(k,l)$ are the phonon frequencies, $e(k,l)$ describes the corresponding atomic displacement, $D(k)$ is the dynamic matrix, which can be obtained from the force constant matrix Φ,

$$D_{st}^{\alpha\beta}(k) = \frac{1}{\sqrt{M_s M_t}} \sum_R \Phi_{st}^{\alpha\beta}(R) \exp(-ikR)\,, \tag{11}$$

where M_s and M_t are masses for atoms s and t, respectively, R is the Bravais lattice vectors. Within the framework of harmonic approximation, keeping only the second terms in the Taylor series of total energy E, Φ is given by

$$\Phi_{st}^{\alpha\beta} = \frac{\partial^2 E}{\partial \mu_s^\alpha \mu_t^\beta}\,, \tag{12}$$

where μ_s^α is the displacement of atom s from its equilibrium position in α direction.

The phonon dispersion and partial phonon densities of states (PDOS) are calculated by using the linear response method within the DFPT.[18]

The wurtzite modification of ZnO, BeO and $Zn_{0.5}Be_{0.5}O$ with the space group C_{6v} and C_{3v}, respectively, has $n = 4$ atoms in the primitive unit cell which leads to $3n = 12$ vibrational eigen modes (3 acoustical and 9 optical modes). Thus, the vibration frequency at the BZ-center $\mathbf{\Gamma}$ point ($q = 0$) is called as a normal vibration mode. The standard group theory analysis yields the following decomposition of the optical vibrational representation in irreducible representation of group C_{6v} and C_{3v}, respectively, at $\mathbf{\Gamma}$ point as follows:

$$\Gamma_{\text{Opt}}^{\text{ZnO}} = 1A_1^{(\text{R+IR})} + 4E_2^{(\text{R})} + 2E_1^{(\text{R+IR})} + 2B_2^{(\text{S})}\,,$$

$$\Gamma_{\text{Opt}}^{\text{BeO}} = 2E_1^{(\text{R+IR})} + 1A_1^{(\text{R+IR})} + 4E_2^{(\text{R})} + 2B_2^{(\text{S})}\,,$$
$$\Gamma_{\text{Opt}}^{\text{Zn}_{0.5}\text{Be}_{0.5}\text{O}} = 6E^{(\text{R+IR})} + 3A_1^{(\text{R+IR})}\,,$$

where IR and R correspond to infrared and Raman active modes, respectively. Here, all modes except B_2 are active in Raman spectra, whereas only those with A_1 and E_1 symmetry are allowed in infrared spectra. Consequently, there are totally three infrared and Raman active modes, four Raman active modes and two silent (S) modes. The remaining nine optical modes contain nine infrared active and Raman active vibration modes ($6E + 3A_1$).

The primitive unit cell of wurtzite $Zn_{0.75}Be_{0.25}O$ and $Zn_{0.25}Be_{0.75}O$ contains 16 atoms with 48 normal modes at the center of the Brillouin zone (BZ), which can be described by the irreducible representations of the point group C_{6v} as follows:

$$\Gamma_{\text{Opt}}^{\text{Zn}_{0.75}\text{Be}_{0.25}\text{O}} = 5A_1^{(\text{R+IR})} + 14E_1^{(\text{R+IR})} + 16E_2^{(\text{R})} + 2A_2^{(\text{S})} + 2B_1^{(\text{S})} + 6B_2^{(\text{S})}\,,$$
$$\Gamma_{\text{Opt}}^{\text{Zn}_{0.25}\text{Be}_{0.75}\text{O}} = 5A_1^{(\text{R+IR})} + 14E_1^{(\text{R+IR})} + 16E_2^{(\text{R})} + 2A_2^{(\text{S})} + 2B_1^{(\text{S})} + 6B_2^{(\text{S})}\,,$$

where the acoustic modes are A_1 and $2E_1$. Over this decomposition, the remaining 45 optical modes contain 19 Raman and infrared active vibration modes, 16 Raman active modes and 10 silent (non-active).

The calculated phonon dispersion curves along several high-symmetry lines in the BZ and the corresponding total and atomic projected partial phonon densities of states are shown in Figs. 1 and 2, respectively. Obviously, the calculated full phonon dispersion relations have no soft modes, i.e. negative frequencies, at any wave vectors, indicating the dynamical stabilities of $Zn_{1-x}Be_xO$ corresponding to $x = 0.0$, 0.25, 0.50, 0.75 and 1.0, respectively.

Table 4 presents the optical phonon frequencies calculated at $\mathbf{\Gamma}$ point for $Zn_{1-x}Be_xO$ corresponding to $x = 0.0$, 0.25, 0.50, 0.75 and 1.0, respectively. Unfortunately, there are no experimental data and theoretical values for comparison for $Zn_{0.75}Be_{0.25}O$, $Zn_{0.5}Be_{0.5}O$ and $Zn_{0.25}Be_{0.75}O$, so our results are predictions, while the phonon frequencies obtained for ZnO and BeO are in good agreement with experimental and theoretical data in Refs. 45–49.

The partial phonon densities of states are displayed in Fig. 2 for better understanding of contributions to the phonon structure of each atom. Generally, the low frequency modes below 310 cm^{-1} are mainly from Zn and the high frequency modes (above 354 cm^{-1}) are dominated by the partial DOS of Be. The partial phonon DOS of $Zn_{1-x}Be_xO$ clearly indicates that Zn atoms contribute more to the low frequency region than Be and O atoms, because of the heavier mass of Zn than the other two atoms. It is interesting to note that there exist overlaps between optical phonons and acoustic phonons in a broad frequency for $Zn_{0.5}Be_{0.5}O$, $Zn_{0.25}Be_{0.75}O$ and BeO. This is different in the case of $Zn_{0.75}Be_{0.25}O$ and ZnO, as there is a phonon band gap at frequency about 72.70 cm^{-1} and 132.32 cm^{-1} for $Zn_{0.75}Be_{0.25}O$ and ZnO, respectively. This can be understood from the atomic

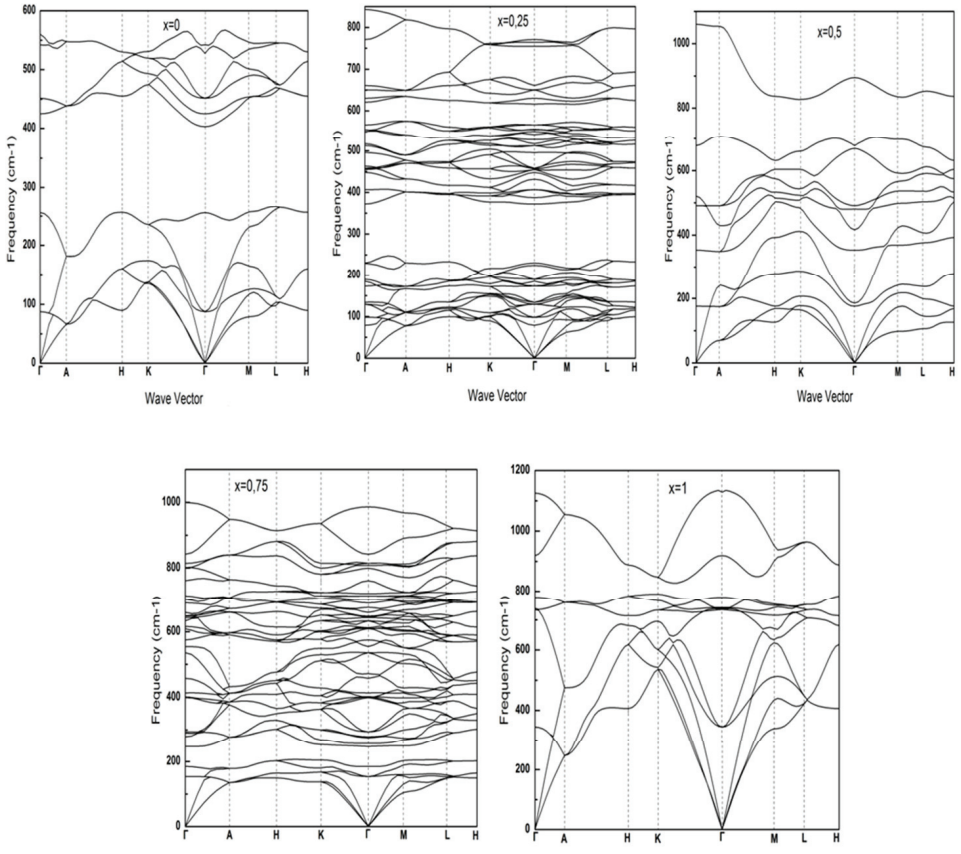

Fig. 1. Calculated phonon dispersion curves along symmetry lines for $Zn_{1-x}Be_xO$.

masses of O, Be and Zn, while the significantly large atomic mass of Zn results in the phonon band gap.

The vibration motions of low-frequency region (≤ 310 cm^{-1}) are mainly related to the translational movements of Zn and O atoms. The vibration motions of E_2 mode at 98.02 cm^{-1} translational movements of Zn and half of O atoms and the Be and half of O atoms are kept still. In addition, the translational vibrations in the high frequency region (≥ 354 cm^{-1}) are mainly related to the movements of Be and O atoms. For the E_1 mode at 371.86 cm^{-1}, the Be and O atoms have translational movements with each other along the y-axis and half of Zn atoms move in the opposite direction along the y-axis.

3.2.2. *Born effective charge tensors*

The Born effective charges for anions and cations at $\mathbf{\Gamma}$ point and for various x content have been calculated using the DFPT method.[18] The resulting Born effective charges tensors of each element are listed in Table 5.

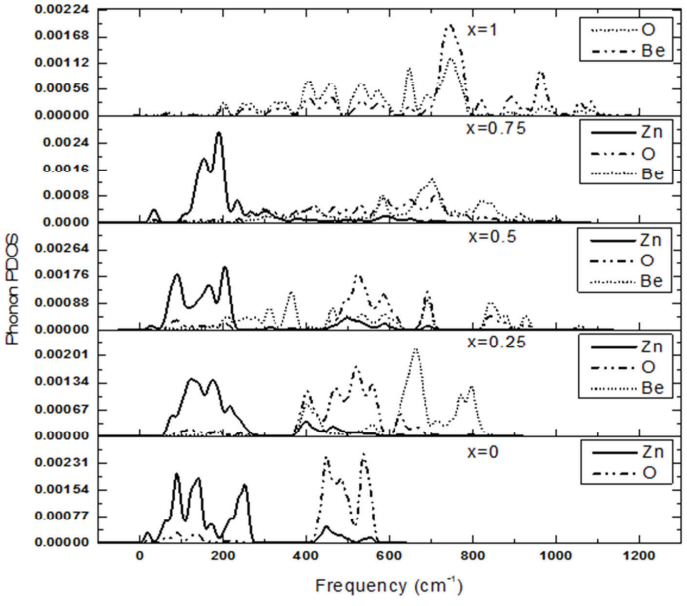

Fig. 2. The calculated partial phonon densities of states for $Zn_{1-x}Be_xO$.

Table 4. Phonon frequencies (cm^{-1}) of $Zn_{1-x}Be_xO$ at Γ point compared with the available experimental data.

ZnO		$Zn_{0.75}Be_{0.25}O$		$Zn_{0.5}Be_{0.5}O$		$Zn_{0.25}Be_{0.75}O$		BeO	
Mode	Raman	Mode	Raman	Mode	Raman	Mode	Raman	Mode	Raman
E_2	87.56	E_2	98.02	E	175.91	E_2	154.13	E_2	344.92
	100[a]	E_1	129.53	E	352.97	E_1	247.09		329.71[d]
A_1	402.92	E_2	134.46	A_1	480.61	A_1	275.57		329.89[d]
	380[a]	E_1	173.06	E	491.21	E_2	294.02		337.3[e]
	379[b]	E_2	189.72	A_1	669.64	E_2	398.48	E_2	733.57
E_1	424.78	A_1	224.56	A_1	894.74	E_1	401.14		658.75[d]
	410[a]	E_1	371.86			E_1	413.15		720.6[d]
	411[b]	A_1	387.47			E_2	535.70		683[e]
E_2	451.38	E_2	406.32			E_1	574.68	A_1	740.91
	438[a]	E_2	454.82			E_2	609.07		658.89[d]
	439[b,c]	E_1	456.71			A_1	610.18		717.79[d]
		E_2	512.24			E_2	632.92		678[e]
		E_1	517.03			E_1	642.65	E_1	779.75
		A_1	542.82			A_1	644.49		699.5[d]
		E_1	549.94			E_2	699.63		757.35[d]
		E_2	566.17			E_1	713.96		722.7[e]
		A_1	616.51			A_1	721.17		
		E_2	650.64			E_1	799.49		
		E_1	661.03			A_1	807.67		
		A_y1	754.87			E_y2	814.28		

[a]Ref. 45, [b]Ref. 46, [c]Ref. 47, [d]Ref. 48, [e]Ref. 49.

[a]Raman data for natural ZnO at 7 K.
[b]Raman data for natural ZnO at room temperature, $B_0 = 143$ GPa.
[c]Raman data for natural ZnO at room temperature, $B_0 = 170$ GPa.

Table 5. Calculated Born effective charge of Zn, Be, O_1 and O_2 for $Zn_{1-x}Be_xO$.

Born effective charge tensors				
ZnO	$Zn_{0.75}Be_{0.25}O$	$Zn_{0.5}Be_{0.5}O$	$Zn_{0.25}Be_{0.75}O$	BeO
O $\begin{pmatrix} -2.41 & 0.00 & 0.00 \\ 0.00 & -2.41 & 0.00 \\ 0.00 & 0.00 & -2.14 \end{pmatrix}$	Be $\begin{pmatrix} 1.97 & 0.00 & 0.00 \\ 0.00 & 1.97 & 0.00 \\ 0.00 & 0.00 & 1.92 \end{pmatrix}$	Be $\begin{pmatrix} 1.84 & 0.00 & 0.00 \\ 0.00 & 1.84 & 0.00 \\ 0.00 & 0.00 & 2.28 \end{pmatrix}$	Be $\begin{pmatrix} 1.89 & 0.00 & 0.10 \\ 0.00 & 1.87 & 0.00 \\ -0.15 & 0.00 & 1.88 \end{pmatrix}$	Be $\begin{pmatrix} 1.76 & 0.00 & 0.00 \\ 0.00 & 1.76 & 0.00 \\ 0.00 & 0.00 & 1.82 \end{pmatrix}$
Zn $\begin{pmatrix} 2.41 & 0.00 & 0.00 \\ 0.00 & 2.41 & 0.00 \\ 0.00 & 0.00 & 2.14 \end{pmatrix}$	O $\begin{pmatrix} -2.16 & 0.00 & 0.11 \\ 0.00 & -1.98 & 0.00 \\ 0.11 & 0.00 & -2.04 \end{pmatrix}$	Zn $\begin{pmatrix} 2.08 & 0.00 & 0.00 \\ 0.00 & 2.08 & 0.00 \\ 0.00 & 0.00 & 1.98 \end{pmatrix}$	O $\begin{pmatrix} -1.81 & 0.00 & -0.12 \\ 0.00 & -1.93 & 0.00 \\ -0.01 & 0.00 & -1.98 \end{pmatrix}$	O $\begin{pmatrix} -1.76 & 0.00 & 0.00 \\ 0.00 & -1.76 & 0.00 \\ 0.00 & 0.00 & -1.82 \end{pmatrix}$
	Zn $\begin{pmatrix} 2.11 & 0.06 & -0.06 \\ 0.06 & 2.04 & 0.11 \\ 0.06 & -0.11 & 2.18 \end{pmatrix}$	O $\begin{pmatrix} -1.99 & 0.00 & 0.00 \\ 0.00 & -1.99 & 0.00 \\ 0.00 & 0.00 & -2.14 \end{pmatrix}$	Zn $\begin{pmatrix} 1.85 & 0.00 & 0.00 \\ 0.00 & 1.85 & 0.00 \\ 0.00 & 0.00 & 2.17 \end{pmatrix}$	
	O $\begin{pmatrix} -1.98 & 0.00 & 0.00 \\ 0.00 & -1.98 & 0.00 \\ 0.00 & 0.00 & -2.35 \end{pmatrix}$	O $\begin{pmatrix} -1.93 & 0.00 & 0.00 \\ 0.00 & -1.93 & 0.00 \\ 0.00 & 0.00 & -1.85 \end{pmatrix}$	O $\begin{pmatrix} -1.89 & 0.00 & 0.00 \\ 0.00 & -1.89 & 0.00 \\ 0.00 & 0.00 & -1.86 \end{pmatrix}$	

The averaged Born effective charges of three main polarized orientations (*xx*, *yy*, *zz*) are 2.32, 2.11, 2.05 and 1.96 for Zn atoms corresponding to $x = 0.0$, 0.25, 0.50 and 0.75, respectively, and the averaged Born effective charge for $O_1(O_2)$ atoms are -2.10 (-2.06), -1.90 (-2.04) and -1.88 (-1.91) corresponding to $x = 0.25$, 0.50 and 0.75, respectively. It is noted that the averaged Born effective charge of O_1 is -2.32 corresponding to $x = 0$, while the averaged Born effective charge of O_2 is -1.78 at $x = 1$. In addition, the averaged Born effective charge of Be is 1.95, 1.99, 1.88 and 1.78 corresponding to $x = 0.25$, 0.50, 0.75 and 1, respectively. We found that the averaged Born effective charge of Zn, Be and O decreased with increasing Be concentration.

The nominal ionic charges of Zn, Be and O are +2, +2 and −2, respectively. The dynamical effective charges of Zn, Be and O are close to their nominal ionic charges, indicating the strong ionization of Zn, Be and O in $Zn_{0.75}Be_{0.25}O$, $Zn_{0.5}Be_{0.5}O$ and $Zn_{0.25}Be_{0.75}O$, respectively. However, the effective charges of Be and O seem to be smaller in magnitude than their nominal charges for BeO, it is found that the values of Z^* of Zn and O are larger than its nominal ionic charge for ZnO, indicating a mixed covalent–ionic bonding. The Born charges on the anion and cation are equal opposite in wurtzite ZnO and BeO, our Z^* values for ZnO and (BeO) agree well with both experimental data -2.10 (-1.85) quoted in Ref. 50 and theoretical data -2.05 (-1.72) quoted in Ref. 51. In the $0 < x < 1$ range, our results born of effective charge are predictions.

3.2.3. *Dielectric permittivity tensors*

The electronic (ε_∞) and static (ε_0) dielectric permittivity tensors and the lattice dielectric constant ε^{lat} at $\mathbf{\Gamma}$ point and for various x content were calculated by LDA, shown in Table 6. The static dielectric tensors are calculated using the dynamic matrix and effective charges, which can be written as follows.[52]

$$\varepsilon_0 = \varepsilon_\infty + \frac{4\pi e^2}{V} \sum \frac{S_m}{\omega_\lambda^2}\,, \tag{13}$$

where V is the volume of the primitive unit cell, ω_λ is the wave number of the mode m, S_m is the mode-oscillator strength tensor, related to the eigen displacements direction and Born effective charge tensors, respectively, while, $\varepsilon_0 - \varepsilon_\infty$ is the lattice dielectric constant ε^{lat}.

From Table 6, the dielectric permittivity tensors just have two independent components: $\varepsilon_\parallel$ along the *c*-axis and $\varepsilon_\perp$ perpendicular to the *c*-axis. We saw from the present calculation that the ε_0 is much larger than the ε_∞, which indicates that the contributions from the lattice vibrations are dominant since the ε_0 can be decomposed into electronic contributions and ionic contributions. Our calculated dielectric constants agree well with the experimental data and theoretical values[53–56] for ZnO and BeO compounds. However, no theoretical or experimental value can be found in literature for $Zn_{0.75}Be_{0.25}O$, $Zn_{0.5}Be_{0.5}O$ and $Zn_{0.25}Be_{0.75}O$. Thus, the present

Table 6. Static ε_0, high frequency ε_∞ and lattice ε_{lat} dielectric constants of $Zn_{1-x}Be_xO$.

Structures	$\varepsilon_\perp^\infty$	$\varepsilon_\parallel^\infty$	$\varepsilon_\perp^0$	$\varepsilon_\parallel^0$	$\varepsilon_\perp^{\text{lat}}$	$\varepsilon_\parallel^{\text{lat}}$
ZnO	3.88	3.96	8.25	8.88	4.37	4.92
	3.70[a]	3.78[a]	7.77[a]	8.91[a]	—	—
$Zn_{0.75}Be_{0.25}O$	4.55	4.50	8.80	8.85	4.25	4.35
$Zn_{0.5}Be_{0.5}O$	4.50	4.28	13.29	7.23	8.79	2.95
$Zn_{0.25}Be_{0.75}O$	3.52	3.57	9.40	7.69	5.88	4.12
BeO	3.14	3.13	6.58	7.22	3.44	4.09
	3.05[b]	3.13[b]	6.94[c]	7.65[c]	—	—

[a]Ref. 53, [b]Ref. 54, [c]Ref. 55.

calculations are considered as predictions. From Table 6, one can note that the high frequency dielectric decreases with increasing Be concentration.

The values of the refractive indexes $n = (\varepsilon_\infty)^{1/2}$ are 2.14, 2.12, 2.07, 1.89 and 1.77 for direction along c-axis and 3.00, 2.13, 2.12, 1.88 and 1.77 for perpendicular to c-axis for $Zn_{1-x}Be_xO$ corresponding to $x = 0.0$, 0.25, 0.50, 0.75 and 1.0, respectively, From these data, one can conclude that the refractive index decreases with increasing Be concentration. It has the values of 2.35, 1.98, 1.91, 1.79 and 1.73 for the above concentrations, respectively. For the binary compound, our results agree with the values of Refs. 57 and 58. There is no theoretical or experimental value of optical phonons for $Zn_{0.75}Be_{0.25}O$, $Zn_{0.5}Be_{0.5}O$ and $Zn_{0.25}Be_{0.75}O$ for comparison with the present calculated results.

4. Conclusion

In this work, we have presented a theoretical analysis of the structural and elastic properties of $Zn_{1-x}Be_xO$ alloys by using norm conserving pseudo-potential method in the framework of the density functional theory within the local density approximation. Our calculated lattice constants, a and c, decreased with an increase in beryllium composition. This phenomenon occurs because the atom radius of beryllium is smaller than that of zinc. In addition, the generalized elastic stability criteria for a hexagonal crystal are well satisfied, indicating that these compounds are mechanically stable. The mechanical properties of B, E and G increase with the increase of Be content, in time we found the Poisson's ratio decreases with increasing of Be content. We can get that the ductility of $Zn_{1-x}Be_xO$ is decreased in comparison with that of ZnO. Our results of the lattice constants, elastic constants, the bulk modulus B and Young's modulus E are in reasonable agreement with the experimental data and theoretical values of $Zn_{1-x}Be_xO$.

The lattice dynamical results regarding the phonon dispersion, partial phonon densities of states, Born effective charges, dielectric permittivity tensors are reported within the framework of density functional perturbation theory. Besides, the phonon frequencies at zone-center $\mathbf{\Gamma}$ point have been analyzed. Also, a phonon

band gap appears when content of Be is at least smaller than 0.25. Calculated phonon dispersions show that $Zn_{1-x}Be_xO$ are dynamically stable (no soft modes). Our results of the Born effective charge tensors exhibit anisotropy. Besides, the static dielectric permittivity ε_0 is much larger than the electronic dielectric permittivity ε_∞, which indicates that the contributions from the lattice vibrations are dominant since the ε_0 can be decomposed into electronic contributions and ionic contributions. The values of the refractive indexes $n = (\varepsilon_\infty)^{1/2}$ decrease with an increase in beryllium composition.

The lack of experimental and theoretical data in $0 < x < 1$ range for the phonon dispersion, the electronic (ε_∞) and static (ε_0) dielectric permittivity tensors, the Born effective charge tensors, our results are predictions. Our results are in reasonable agreement with the experimental data and theoretical values for ZnO and BeO.

References

1. Z. L. Wang, *ACS Nano* **2** (2008) 1987–1992.
2. T. S. Ko, T. C. Lu, L. F. Zhuo, W. L. Wang, M. H. Liang, H. C. Kuo, S. C. Wang, L. Chang and D. Y. Lin, *J. Appl. Phys.* 108 (2010) 073504.
3. B. Laumer, T. A. Wassner, F. Schuster, M. Stutzmann, J. Schormann, M. Rohnke, A. Chernikov, V. Bornwasser, M. Koch, S. Chatterjee and M. Eickhoff, *J. Appl. Phys.* **110** (2011) 093513.
4. L. Dong and S. P. Alpay, *J. Appl. Phys.* **111** (2012) 113714.
5. H. Matsui and H. Tabata, *Appl. Phys. Lett.* **98** (2011) 261902.
6. T. Makino, C. H. Chia, N. T. Tuan, Y. Segawa, M. Kawasaki, A. Ohtomo, K. Tamura and H. Koinuma, *Appl. Phys. Lett.* **77** (2000) 1632.
7. F. T. Kong and H. R. Gong, *Comput. Mater. Sci.* **61** (2012) 127e33.
8. Y. Chen, N. W. Emanetoglu, G. Saraf, P. Wu, Y. Lu, A. Parekh, V. Merai, E. Udovich, D. Lu, D. S. Lee, E. A. Armour and M. Pophristic, *IEEE Trans. Ultrason. Ferroelect. Freq. Contr.* **52** (2005) 1161.
9. N. W. Emanetoglu, G. Patounakis, S. Liang, C. R. Gorla, R. Wittstruck and Y. Lu, *IEEE Trans. Ultrason. Ferroelect. Freq. Contr.* **48** (2001) 1389.
10. W. Kohn and L. Sham, *Phys. Rev. A* **140** (1965) 1133.
11. M. D. Segall, P. J. D. Lindan, M. J. Probert, C. J. Pickard, P. J. Hasnip, S. J. Clark and M. C. Payne, *J. Phys.: Condens. Matter* **14** (2002) 2717.
12. P. L. Mao, B. Yu, Z. Liu, F. Wang and Y. Ju, *J. Magn. Alloy* **1** (2013) 256.
13. D. M. Ceperley and B. J. Alder, *Phys. Rev. Lett.* **45** (1980) 566.
14. J. P. Perdew and A. Zunger, *Phys. Rev. B* **23** (1981) 5048.
15. D. R. Hamann, M. Schluter and C. Chiang, *Phys. Rev. Lett.* **43** (1979) 1494–1497.
16. H. J. Monkhorst and J. D. Pack, *Phys. Rev. B* **13** (1976) 5188.
17. B. G. Pfrommer, M. Côté, S. G. Louie and M. L. Cohen, *J. Comp. Physiol.* **131** (1997) 133–140.
18. S. Baroni, S. de Gironcoli, A. D. Corso and P. Giannozzi, *Rev. Mod. Phys.* **73** (2001) 515–562.
19. F. Decremps, F. Datchi, A. M. Saitta, A. Polian, S. Pascarelli, A. D. Cicco, J. P. Itie and F. Baudelet, *Phys. Rev. B* **68** (2003) 104101.
20. A. Schleife, F. Fuchs, J. Furthmüller and F. Bechstedt, *Phys. Rev. B* **73** (2006) 245212.
21. Y. Zheng, Z. Chen, Y. Lu, Q. Wu, Z. Weng and Z. Huang, *J. Semicond.* **29**(12) (2008) 2316–2321.
22. R. M. Hazen and L. W. Finger, *J. Appl. Phys.* **59** (1986) 3728.

23. M. Born and K. Huang, *Dynamical Theory of Crystal Lattices* (Oxford University Press, London, 1954).
24. M. S. Islam and A. K. M. A. Islam, *Physica B* **406** (2011) 275.
25. M. Marlo and V. Milman, *Phys. Rev. B* **62** (2000) 2899.
26. B. Kocak, Y. O. Ciftci, K. Colakoglu and E. Deligoz, *Physica B* **405** (2010) 4139.
27. H. C. Chen and L. J. Yang, *Physica B* **406** (2011) 4489.
28. Z. M. Sun, S. Li, R. Ahuja and J. M. Schneider, *Solid State Commun.* **129** (2004) 589.
29. Z. J. Lin, Y. C. Zhou and M. S. Li, *J. Mater. Sci. Technol.* **23** (2007) 721.
30. R. Hill, *Proc. Phys. Soc.* **65** (1952) 350.
31. G. Carlotti, D. Fioretto, G. Socino and E. Verona, *J. Phys.: Condens. Matter* **7** (1995) 9147.
32. S. Saib and N. Bouarissa, *Phys. Status Solidi B* **244** (2007) 1063–1069.
33. P. Gopal and N. A. Spalpin, *J. Electron. Mater.* **35** (2006) 538–542.
34. Y.-F. Duan, H.-L. Shi and L.-X. Qin, *Phys. Lett. A* **372** (2008) 2930–2933.
35. F. Wang, J. Wu, C. Xia, C. Hu, C. Hu, P. Zhou, L. Shi, Y. Ji, Z. Zheng and X. Liu, *J. Alloys Compd.* **597** (2014) 50–57.
36. O. Madelung (ed.), *Semiconductors: Data Handbook*, 3rd edn. (Springer, Berlin, 2004).
37. Z. Liu, X. He, Z. Mei, H. Liang, L. Gu, X. Duan and X. Du, *J. Phys. D: Appl. Phys.* **47** (2014) 105303.
38. V. Milmanl and M. C. Warren, *J. Phys.: Condens. Matter* **13** (2001) 241.
39. S. O. Kucheyev, J. E. Bradby, J. S. Williams, C. Jagadish and M. V. Swain, *Appl. Phys. Lett.* **80** (2002) 956.
40. Y. Gao and Z. L. Wang, *Nano Lett.* **9** (2009) 1103–1110.
41. G. G. Bentle, *J. Nucl. Mater.* **6**(3) (1962) 336–337.
42. S. F. Pugh, *Philos. Mag.* **45** (1954) 823.
43. J. Y. Wang, Y. C. Zhou, T. Liao and Z. J. Lin, *Appl. Phys. Lett.* **89** (2006) 021917.
44. E. Kaxiras, *Atomic and Electronic Structure of Solids* (Cambridge University Press, New York, 2003).
45. J. Serrano, A. H. Romero, F. J. Manjón, R. Lauck, M. Cardona and A. Rubio, *Phys. Rev. B* **69** (2004) 094306.
46. F. J. Manjón, K. Syassen and R. Lauck, *High Press. Res.* **22** (2002) 299.
47. F. Decremps, J. Pellicer-Porres, A. M. Saitta, J.-C. Chervin and A. Polian, *Phys. Rev. B* **65** (2002) 092101.
48. F. Luo, Y. Cheng, L.-C. Cai and X.-R. Chen, *J. Appl. Phys.* **113** (2013) 033517.
49. A. Bosak, K. Schmalzl, M. Krisch, W. van Beek and V. Kolobanov, *Phys. Rev. B* **77** (2008) 224303.
50. R. M. Martin, *Phys. Rev. B* **5** (1972) 1607.
51. A. Dal Corso, M. Postenak, R. Resta and A. Baldereschi, *Phys. Rev. B* **50**(10) (1994) 715.
52. X. Gonze, *Phys. Rev. B* **55** (1997) 10337–10354.
53. N. Ashkenov *et al.*, *J. Appl. Phys.* **93** (2003) 126.
54. Z.-C. Guo, F. Luo, G.-F. Ji, L.-C. Cai and Y. Cheng, *Physica B* **438** (2014) 60–64.
55. E. Loh, *Phys. Rev.* **166** (1968) 673.
56. M. Posternak, A. Baldereschi, A. Catellani and R. Resta, *Phys. Rev. Lett.* **64** (1990) 1777.
57. B. Lü, X. Zhou, R.-F. Linghu, X.-L. Wang and X.-D. Yang, *Chin. Phys. B* **20**(3) (2011) 036104.
58. T. S. Yen, C. K. Kuo, W. L. Han, Y. H. Qui and Y. Z. Huang, *J. Am. Ceram. Soc.* **66** (1983) 860.